

## **A novel differential ion mobility device expands the depth of proteome coverage and the sensitivity of multiplex proteomic measurements**

### **Authors & Affiliations**

Sibylle Pfammatter<sup>1,2</sup>, Eric Bonneil<sup>1</sup>, Francis P. McManus<sup>1</sup>, Satendra Prasad<sup>3</sup>, Derek

J Bailey<sup>3</sup>, Michael Belford<sup>3</sup>, Jean-Jacques Dunyach<sup>3</sup>, and Pierre Thibault<sup>1,2\*</sup>

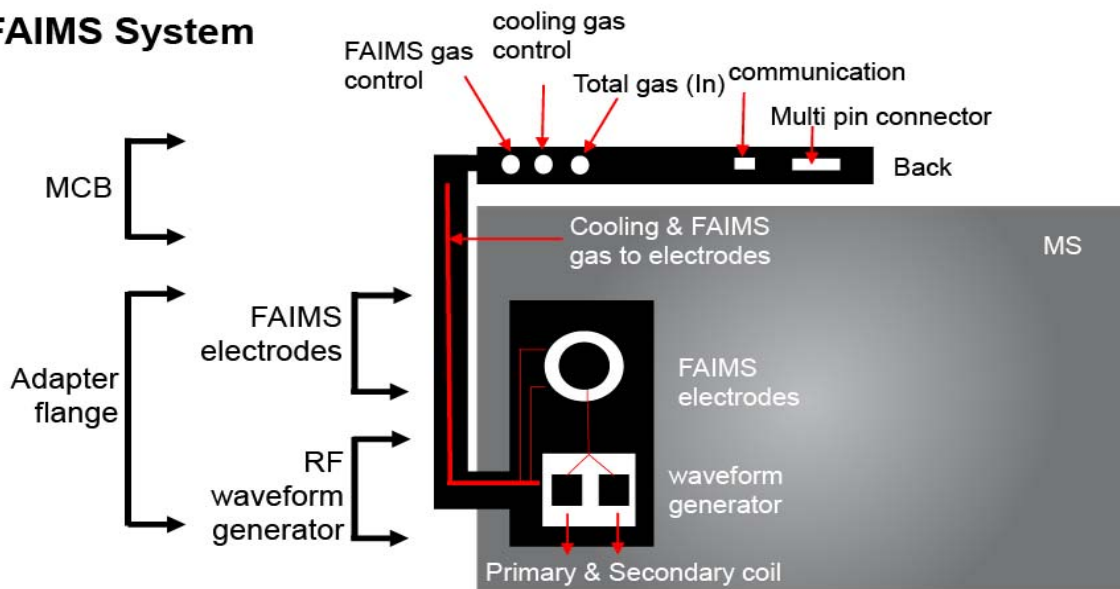
<sup>1</sup>Institute for Research in Immunology and Cancer, H3T 1J4, Québec, Canada

<sup>2</sup>University of Montréal, Department of Chemistry, H3T 1J4, Québec, Canada

<sup>3</sup>Thermo Fisher Scientific, San Jose, California 95134, United States

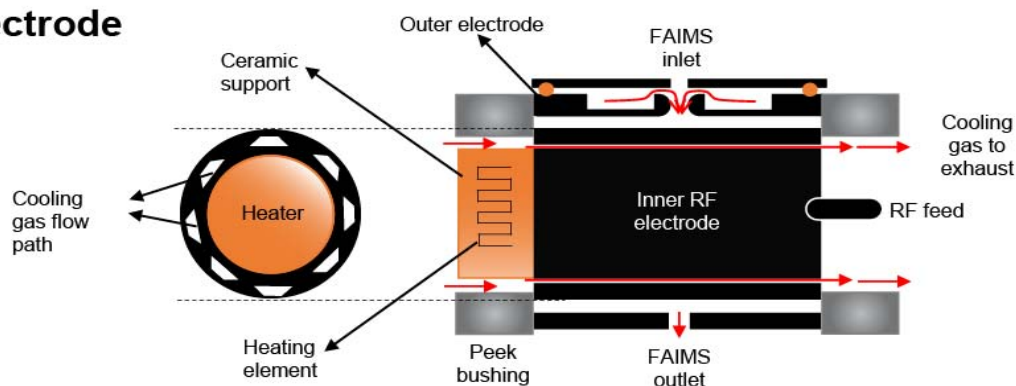
a

### FAIMS System



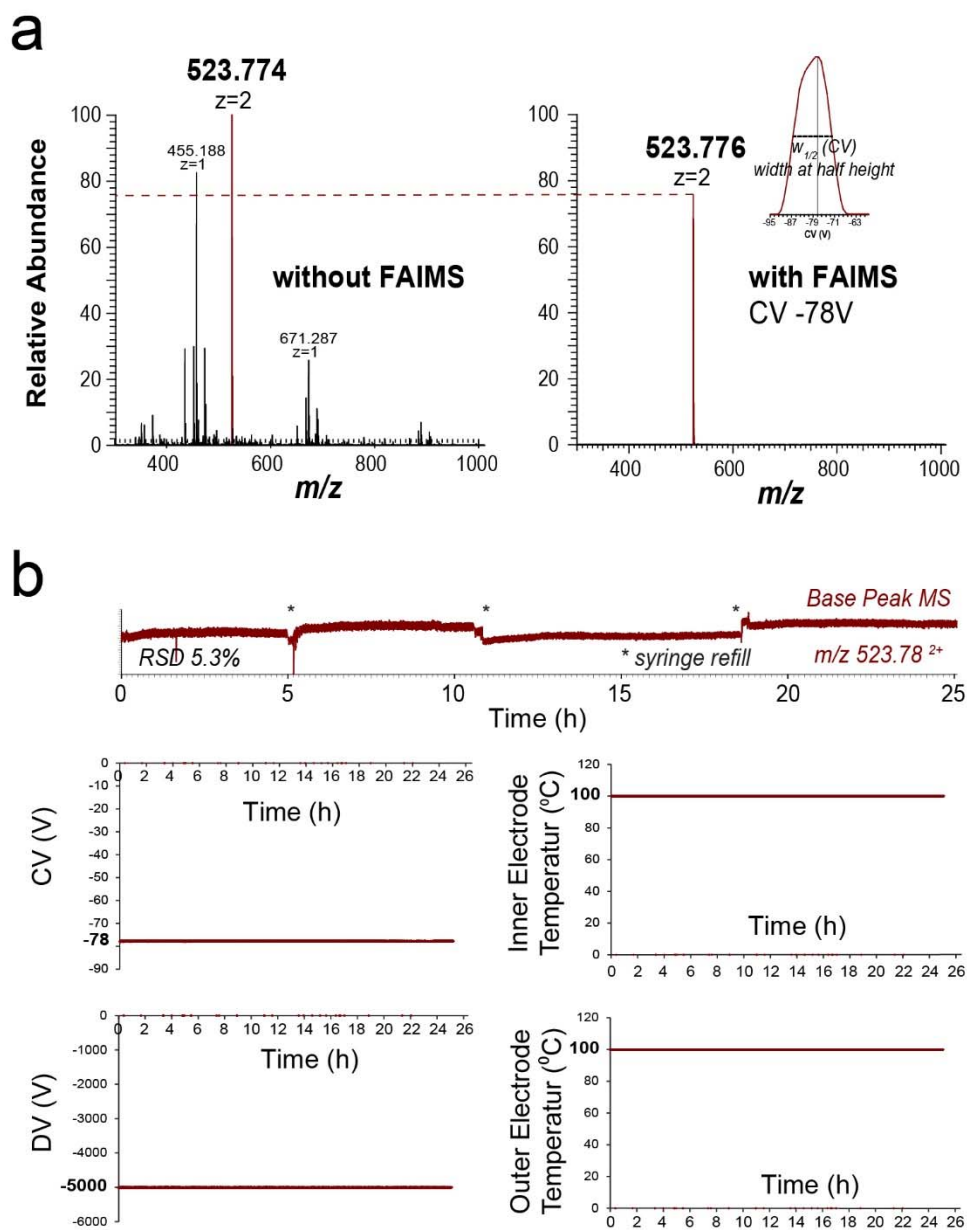
b

### FAIMS Electrode

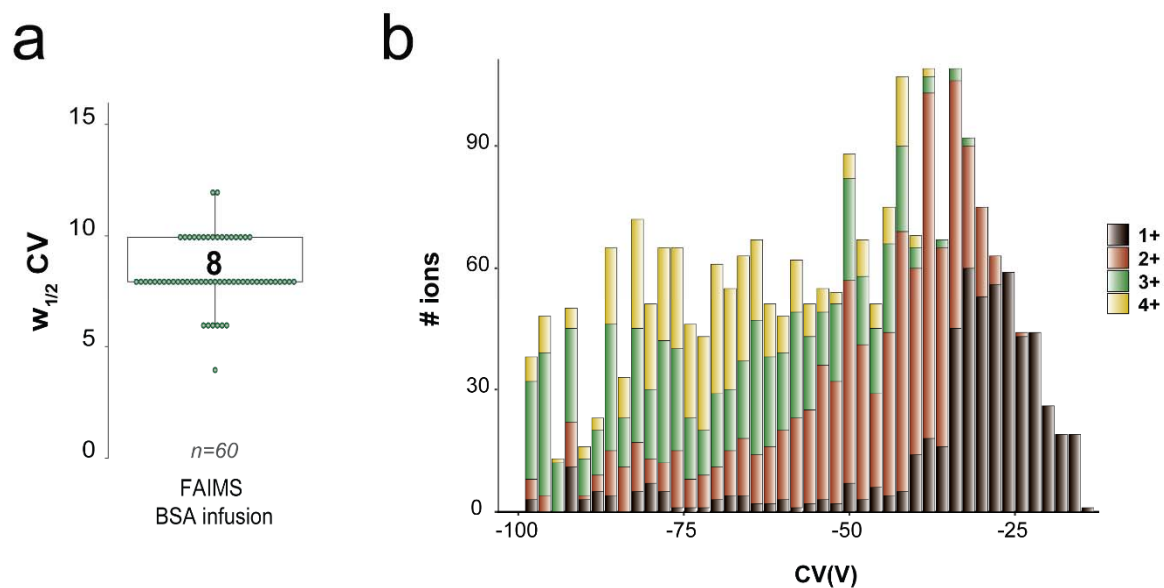


**Supplementary Figure 1:** Schematic of the new FAIMS interface. a) FAIMS interface with Main Control Board (MCB) and an adapter flange that include a RF waveform generator and FAIMS electrodes. The FAIMS electrode sub assembly contain an inner electrode, outer electrode, entrance plate, and three heaters: one for inner electrode and two for outer electrode. The MCB provides multiple DC drive voltages, gas controls, FAIMS electrode heaters and temperature sensors, and a separate supply drives the primary and secondary RF coils to produce +/-5000V ion separation voltage. Other DC voltages in the MCB include voltage for CV and Entrance Plate. An industrial grade N<sub>2</sub> supply is delivered into two separate gas valves used to supply the FAIMS ion transport gas and the electrodes' cooling gas. All DC voltages and two ¼" Teflon tubing gas lines (ion transport and cooling gas) are routed through a "side arm" cable structure. Gas and DC connections to the electrodes were concealed in the adapter flange eliminating the need for user

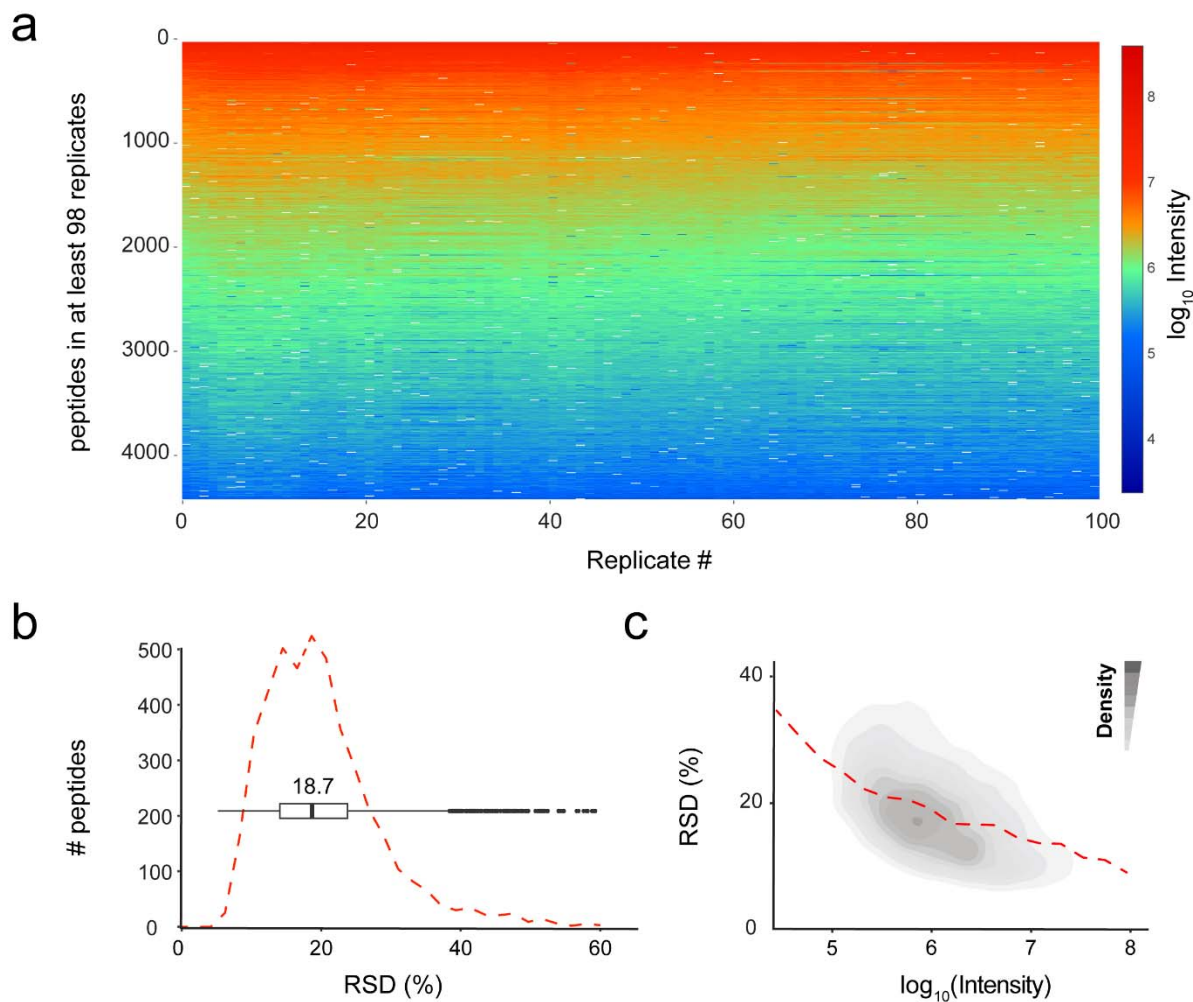
intervention to connect/disconnect the DC voltage and gas lines when alternating between with and without FAIMS experiments. A single task of detaching the adapter flange from the MS restores the system to a “without FAIMS” state and a reverse step restores the MS system to a “with FAIMS” state within seconds. b) Cross section of the FAIMS electrode assembly. A heater block is pressed against one end of the inner electrode to promote conduction of heat transfer. The inner electrode can also be rapidly cooled by disabling the heater and forcing air flow through multiple narrow slits bored in the inner electrode. The cooling air flow is separated from the ion transport flow using peek bushings fitted with vacuum sealing O rings. The ion transport flow is delivered using a separate supply line into an air gap between the outer electrode and the entrance plate. The entire assembly in Figure B is pressed into a cap shaped entrance plate that is easily retractable by releasing tool free latches and sliding the assembly from the adapter flange.



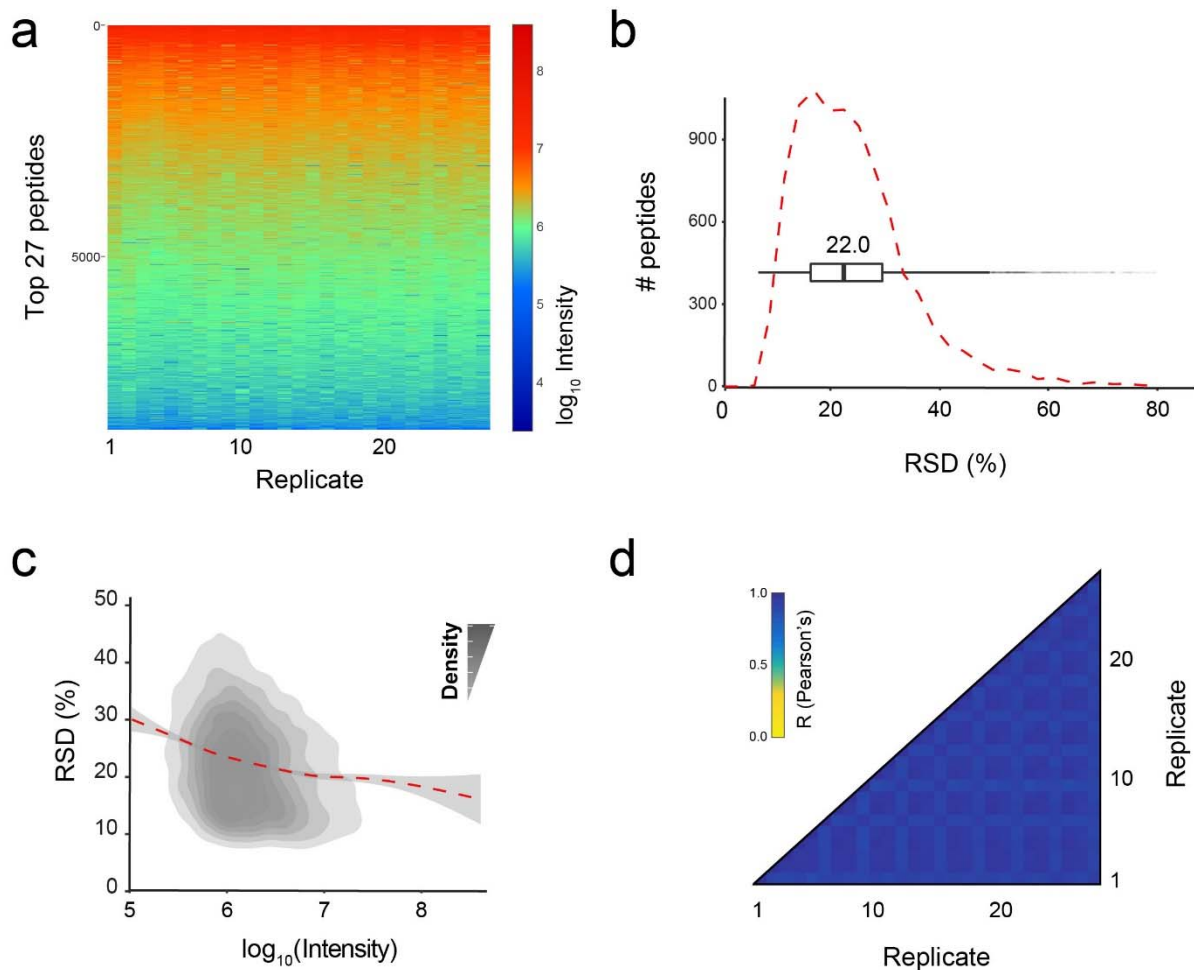
**Supplementary Figure 2:** Ion transmission and stability of the new FAIMS prototype by direct infusion of Angiotensin II. (a) Angiotensin II peptide  $m/z$  523.77<sup>2+</sup> infusion with (left) regular ESI-MS and (right) ESI-FAIMS-MS at the optimal transmission CV of -78V, showing an ion transmission of almost 80 %. (b) Top, Angiotensin II infusion over 24 h with relative standard deviation of signal intensity of 5.3 %. Deviations in the CV voltage (-78V), DV voltage (-5000V) and both inner and outer electrode temperatures (100 °C) over the course of 24 h.



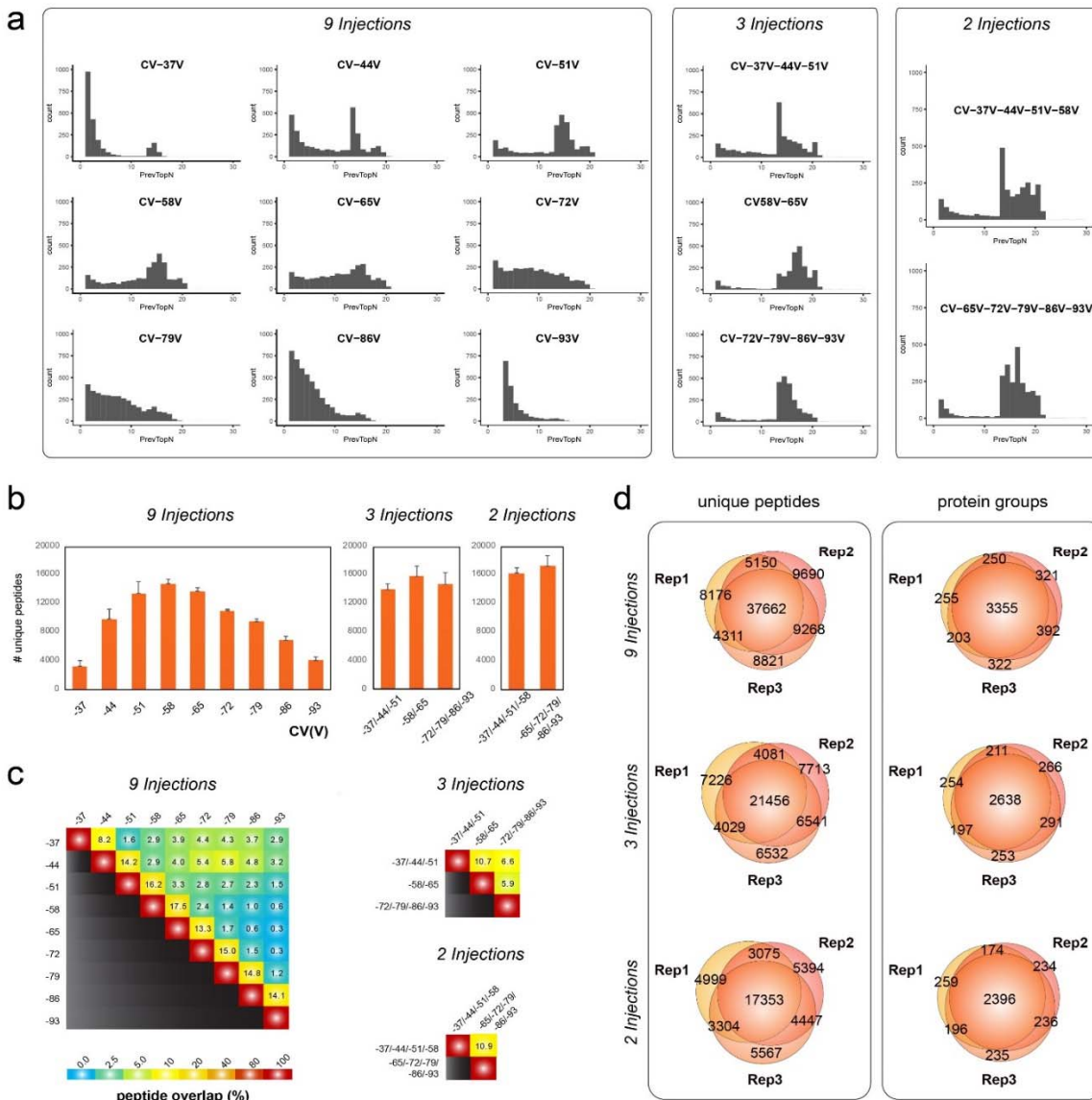
**Supplementary Figure 3:** Resolution of the FAIMS interface using a BSA tryptic digest as benchmark. (a) Boxplot with data spread of the ions from a BSA tryptic digest over the FAIMS CV transmission range showing a median resolution (width at half height) of 8 V. Each green circle represents a different BSA tryptic peptide. (b) Distributions of ion charge states as a function of the FAIMS CV investigated.



**Supplementary Figure 4:** Reproducibility and robustness of FAIMS-Fusion LC-MS system. 100 replicate injections of 500 ng HEK293 digest at a fixed CV (CV -45 V) were continuously monitored over 5 days. (a) Heat map representation of the intensity of the 4427 peptides that were present in 98 % of the injections across the 100 replicates. (b) Relative standard deviation distribution for the corresponding peptides. (c) Plot of the relative standard deviation as a function of ion intensity.

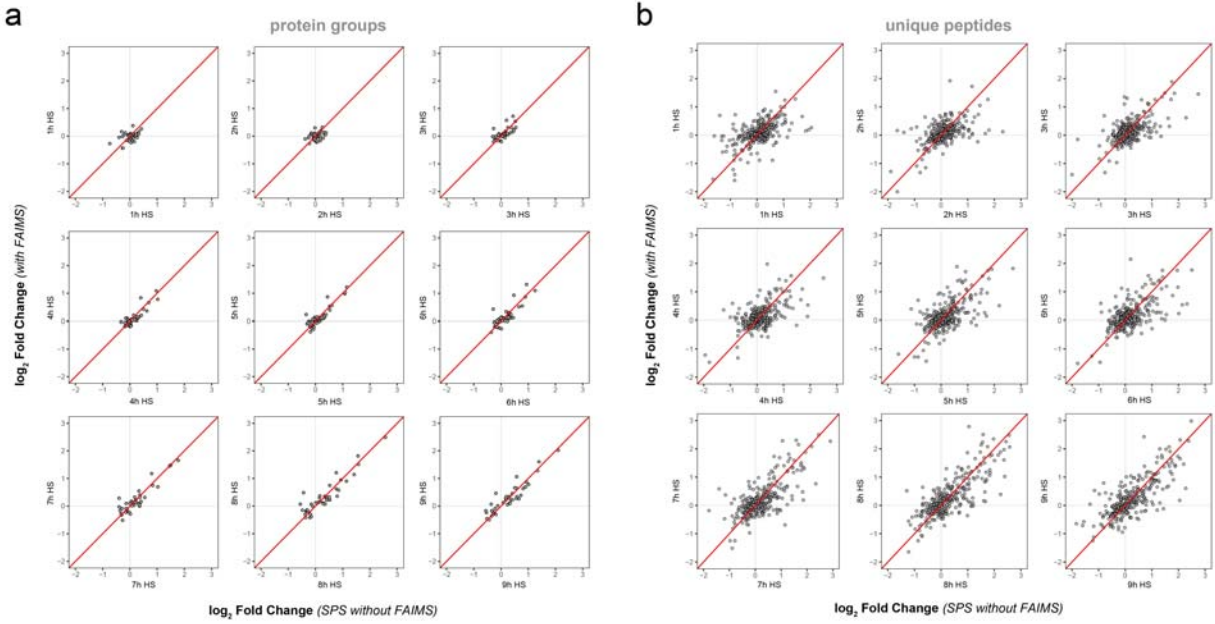


**Supplementary Figure 5:** Reproducibility and robustness of regular LC-MS system with 27 replicate injections of HEK293 digest. (a) Heat map representation of the intensity of the 9225 peptides (total of 42511 peptides) that were present in all 27 replicate injections. (b) Relative standard deviation distribution for the common peptides from the 27 replicate injection with a median of 22.0 %. (c) Plot of RSD as a function of  $\log_{10}$  Intensity for all common peptides. (d) Heat map for Pearson correlation coefficients between all 27 replicate injections.

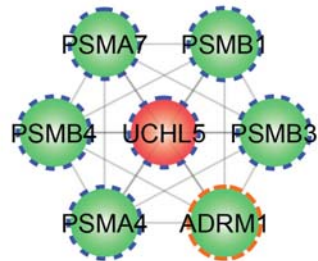
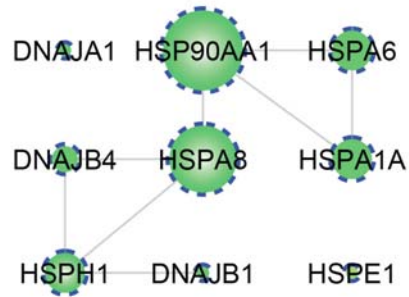
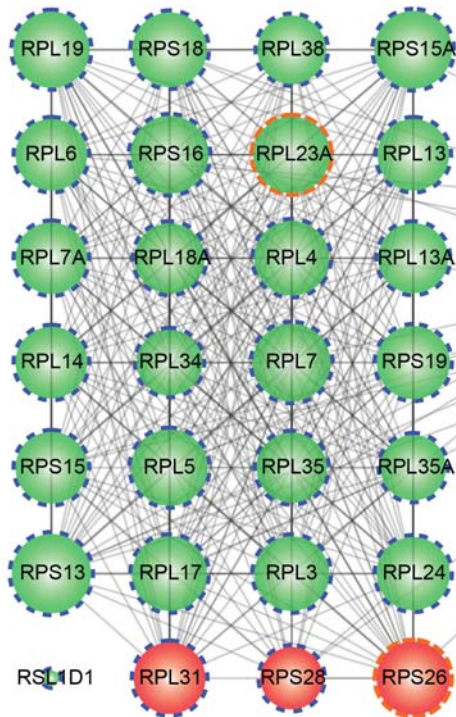
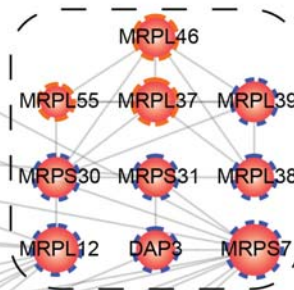


**Supplementary Figure 6:** Optimization of FAIMS CV stepping program. HEK293 digests were analyzed with FAIMS with CV from -37 V to -93 V with 7 V steps to cover the entire peptide transmission range. (a) Duty cycle usage was monitored by following the number of MS<sup>2</sup> triggered per survey scan for (left) 9 injections at individual CV, (middle) 3 injections combining CV-37 V/-44 V/-51 V, CV-58 V/-65 V and CV-72 V/-79 V/-86 V/-93 V and (right) 2 injections combining CV-37 V/-44 V/-51 V/-58 V and CV-65 V/-72 V/-79 V/-86 V/-93 V. (b) Number of unique peptide sequences identified per injection for (left) individual CV, (middle) 3 injection combination and (right) 2 injection combination. (c) Heat map representation of the overlap in peptide identification between the various injections. (d) Overlap of three technical replicates for (top) individual CV, (middle) 3 injection combination and (bottom) 2 injection combination. The overlap for the number of (left) unique peptides and (right) protein groups ( $\geq 2$  unique peptides/protein) are depicted in the Venn diagrams.





**Supplementary Figure 7:** Comparison between SPS and FAIMS based TMT quantifications. Scatterplot representations for the common dynamic (a) proteins and (b) peptides that changed in abundance during the heat shock response in HEK293 cells. Scatterplots correspond to each of the 9 time points investigated.

**a****Proteasome complex****b****Response to unfolded protein****c****Cytoplasmic Ribosome****Mitochondrial Ribosomes**

Late

Early

**Supplementary Figure 8:** The heat shock response affects proteins with similar functions in the same demeanor. Sub networks were extracted from the protein network shown in Figure 7a based on their enriched GO-term. Proteins outlined in blue display a delayed response (>1 h) and proteins outlined in orange displayed acute responses (<1 h). Red nodes depict proteins whose abundances decreased in response to the heat shock, while green nodes depict proteins whose abundances increased. Proteins from the same sub network changed abundance with similar dynamics. (a) Proteasome complex sub network. (b) Response to unfolded protein sub network. (c) Ribosome sub network.